Heliyon 7 (2021) e06723

Contents lists available at ScienceDirect

Heliyon

journal homepage: www.cell.com/heliyon

Research article

# Optimising the computational domain size in CFD simulations of tall buildings

Yousef Abu-Zidan *, Priyan Mendis, Tharaka Gunawardena

*Department of Infrastructure Engineering, The University of Melbourne, VIC 3010, Australia*

ARTICLE INFO

*Keywords:*
Computational domain
Tall buildings
CFD simulation
Wind loading
Venturi effect

ABSTRACT

Recently, there has been a growing interest in utilizing computational fluid dynamics (CFD) for wind resistant design of tall buildings. A key factor that influences the accuracy and computational expense of CFD simulations is the size of the computational domain. In this paper, the effect of the computational domain on CFD predictions of wind loads on tall buildings is investigated with a series of sensitivity studies. Four distinct sources of domain error are identified which include wind-blocking effects caused by short upstream length, flow recirculation due to insufficient downstream length, global venturi effects due to large blockage ratios, and local venturi effects caused by insufficient clearance between the building and top and lateral domain boundaries. Domains based on computational wind engineering guidelines are found to be overly conservative when applied to tall buildings, resulting in uneconomic grids with a large cell count. A framework for optimizing the computational domain is proposed which is based on monitoring sensitivity of key output metrics to variations in domain dimensions. The findings of this paper help inform modellers of potential issues when optimizing the computational domain size for tall building simulations.

## 1. Introduction

The use of computational fluid dynamics (CFD) for wind resistant design of tall buildings has gained interest in recent years as advancement in computing power has made solving complex flow problems increasingly affordable. A key factor that influences the accuracy and cost of CFD simulations is the size of the computational domain.

The computational domain (Figure 1) refers to an external volumetric region that surrounds the building model, where the basic flow equations are discretised and solved. A total of six boundaries define the extents of a typical domain of cuboid shape. Aside from the bottom of the domain, these boundaries are mostly non-physical, so their influences on the flow region constitute a source of error in the simulation (hereby termed *domain errors*). Non-physical boundaries should be placed far enough from the building to avoid significant influences on the results. However, placing the boundaries too far could increase the computational cost of the model. Consideration for both computational cost and solution accuracy dictates the need for optimizing the size of the computational domain.

The importance of an adequately sized computational domain for solution accuracy is recognized by computational wind engineering (CWE) best practice guidelines (Blocken, 2015; Franke et al., 2007; Tominaga et al., 2008). These guidelines attribute domain errors to comparable issues in wind tunnel testing such as blockage effects in domains of small cross-sectional area, and artificial acceleration of local flow in domains with inadequate clearance between the building model and domain boundaries. Hence, sizing requirements are specified in terms of maximum blockage ratios, minimum distances between the domain boundaries and the building model, or a combination of both (Blocken, 2015).

Franke et al. (2007) recommend a maximum blockage ratio of 3% based on an early study of domain effects in wind load predictions of a low-rise building (Baetke et al., 1990). A similar limit on blockage ratio is recommended by Tominaga et al. (2008) for pedestrian wind comfort studies around tall buildings, although this was justified based on experience from wind tunnel testing. In addition to the blockage ratio, Franke et al. (2007) impose minimum upstream, downstream, and lateral distances of $5H$, $15H$ and $\pm 5H$, respectively, where $H$ is the height of the tallest building in the model. These distances were derived from earlier studies that were a part of a multi-partner project that evaluated uncertainties in CFD modelling of pollutant dispersion around buildings (Castro et al., 1999; Cowan et al., 1997; Hall, 1997). Tominaga et al.

* Corresponding author.
*E-mail address:* yabuzidan@unimelb.edu.au (Y. Abu-Zidan).

https://doi.org/10.1016/j.heliyon.2021.e06723
Received 11 June 2020; Received in revised form 20 December 2020; Accepted 1 April 2021

(2008) recommend similar upstream and lateral distances but specify a shorter downstream length of 10*H*.

While these guidelines are sufficient for preventing domain effects in most CWE applications (Blocken, 2015), they were found to be overly conservative when applied to tall buildings (Revuz et al., 2012). Many studies of tall buildings use smaller domains than those recommended above, but there is little consistency between the domain sizes used in such studies [e.g. (Braun and Awruch, 2009; Huang et al., 2007, 2011; Ricci et al., 2018; Zhang et al., 2015)].

For CFD simulations of wind loading on tall buildings, domain optimization is necessary because it can greatly impact the computational cost. Tall buildings are governed by dynamic wind effects such as crosswind vibrations due to vortex shedding, and simulating these effects requires the use of scale-resolving simulations which require high grid refinement throughout the domain. High refinement is particularly needed in the upstream region to accurately transport inflow turbulence from the inlet boundary to the location of the building. Because of the high grid refinement, the size of the computational domain will greatly influence the cell count in the model. Moreover, even if optimizing the domain only achieves a modest reduction in cell count, savings in computational cost would accrue in a transient simulation over thousands of timesteps.

Optimal domain sizing is difficult to codify because it is highly problem-specific. However, a basic investigation into the nature of domain errors and their impact on the results would greatly help in guiding the optimization process. To our knowledge, no such study has been performed for tall building applications. Furthermore, domain studies in the literature do not demonstrate horizontal homogeneity of the atmospheric boundary layer (ABL) which is needed to provide confidence that domain errors are investigated independently of ABL inhomogeneity errors since both domain errors and ABL inhomogeneity errors are sensitive to upstream domain length (Abu-Zidan et al., 2020). Many studies do not address the issue at all (Buccolieri and Di Sabatino, 2007; Ramponi and Blocken, 2012; Xiang and Wang, 2007), while others acknowledge this issue but do not quantify its impact on their findings (Ai and Mak, 2015; Revuz et al., 2012).

To address these limitations, this paper will investigate the effect of the computational domain size in CFD simulations of wind loading on tall buildings with a series of sensitivity studies that include examining the effect of (1) domain dimensions and (2) blockage ratio, as well as the influence of (3) additional parameters of wind speed and geometric scale. The first two studies involve a direct investigation of domain effects on wind load predictions. Domain parameters are varied in isolation to help identify various sources of domain error in the simulation. The third sensitivity study is performed to generalise the findings from studies 1 and 2 to cases of various wind speeds and geometric scales. Moreover, the study will demonstrate the achievement of a horizontally homogenous ABL, which will ensure that domain errors are investigated in isolation. The findings of this paper will help inform modellers of potential issues when optimizing the computational domain size for tall building simulations.

## 2. Analysis cases and numerical setup

In this paper, domain investigations are performed for a generic rectangular tall building with full-scale dimensions of 40 m in both width (*B*) and depth (*D*), and 200 m in height (*H*). The size of the computational domain is defined by four variables; $l_u$, $l_d$, $b$, and $h$ (see Figure 1); where $l_u$ is the upstream domain length from the inlet to the windward building face, $l_d$ is the downstream length from the leeward building face to the outlet plane, $b$ is the side clearance on either side of the building, and $h$ is the total height of the domain.

This paper consists of three distinct studies, each comprising several simulation cases. In the first study, the domain extents $l_u$, $l_d$, $b$, and $h$ are each varied independently to assess the impact of each of these parameters in isolation. In the second study, the impact of the blockage ratio (*BR*) is investigated by varying $b$ and $h$ simultaneously. Finally, in the third study, the impact of wind speed and geometric scale on domain errors is examined. Details of the simulation cases for each of the three studies are summarized in Table 1.

The domain dimensions shown in Table 1 with a single asterisk (*) are based on the commonly adopted guidelines by Franke et al. (2007) and are henceforth referred to as the base case (BC). Simulation cases are constructed by altering the parameters of interest from the BC, while the other parameters remain at the BC values. Most of the domain sizes in Table 1 are selected to be smaller than the BC since the BC is conservatively large for the tall building in this study. Nonetheless, for each of studies 1 and 2, at least one case is selected to be significantly larger than the BC. This large case is assumed to represent an infinitely large domain that is free from domain errors.

### 2.1. Demonstrating ABL homogeneity

To investigate the nature of domain errors, it is important to ensure that these errors act in isolation. A potential secondary source of error in the current study is due to ABL inhomogeneity. ABL inhomogeneity refers to an unintended adaptation in the ABL profile often caused by an incompatibility of the inlet profile equations with the turbulence model and near-wall functions. Controlling ABL inhomogeneity in this study is important because both ABL inhomogeneity errors and domain errors are influenced by upstream domain length $l_u$. A fuller discussion of the relationship between ABL inhomogeneity errors and upstream domain length has been presented by Abu-Zidan et al. (2020).

ABL homogeneity is achieved by ensuring that flow continuity equations are in balance with the turbulence model that is adopted in the

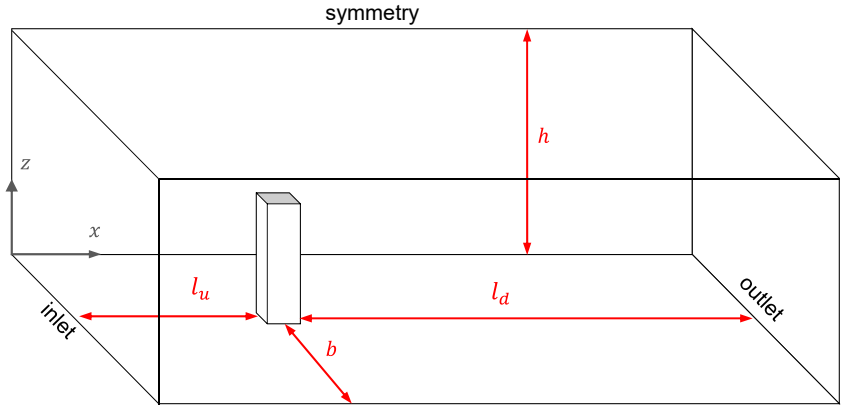


**Figure 1.** Computational domain dimensions and boundary conditions.

**Table 1.** Details of simulation cases for sensitivity studies in this paper.

| Sensitivity study | 1. Impact of domain extents | | | | 2. Impact of blockage ratio | 3. Impact of wind speed and geometric scale | |
|---|---|---|---|---|---|---|---|
| Parameter | $l_u$ | $l_d$ | $b$ | $h$ | $BR$ | Wind speed | Geometric scale |
| Simulation cases | $1H$ | $3H$** | $1.5H$ | $2.2H$ | 2.16% ($b = 2H$, $h = 2.2H$) | $U_{ref} = 10$ m/s (OD**) | 1:400 (OD) |
| | $1.5H$ | $5H$ | $2H$ | $3H$ | 1.59% ($b = 2H$, $h = 3H$) | | |
| | $2H$ | $8H$ | $3H$** | $4H$** | 1.28% ($b = 2.5H$, $h = 3H$) | | |
| | $3H$** | $10H$ | $4H$ | $6H$* | 0.81%** ($b = 3H$, $h = 4H$) | $U_{ref} = 10$ m/s (BC) | 1:400 (BC) |
| | $4H$ | $15H$* | $5H$* | $8H$ | 0.33%* ($b = 5H$, $h = 6H$) | | |
| | $5H$* | $20H$ | $7H$ | $10H$ | 0.10% | | |
| | $7H$ | $25H$ | $10H$ | | ($b = 10H$, $h = 10H$) | | |
| | $10H$ | | | | | | |

* Dimensions of base case (BC) based on recommendations by Franke et al. (2007).
** Optimised domain (OD) selected based on findings from analyses 1 and 2.

simulation, the ABL profiles that are specified at the inlet, and the wall function that replicates roughness conditions at the ground. At the inlet boundary, theoretical ABL profiles are specified based on expressions derived by Richards and Norris (2011) [Eqs. (1), (2), and (3)] that are in balance with the RNG $k$-$\epsilon$ turbulence model adopted in this study. A driving shear stress is specified at the top boundary [Eq.(4)], and a modified wall function proposed by Parente et al. (2011) is applied to the ground. The modified wall function is based on aerodynamic roughness height $z_0$ and can accurately produce ground roughness conditions that are necessary for maintaining homogeneity of the ABL. Full details for this modelling approach can be found in a previous study by the authors (Abu-Zidan et al., 2020).

$$U = \frac{u_*}{\kappa} \ln\left(\frac{z + z_0}{z_0}\right);\ C_\mu = 0.085; \kappa = 0.4 \tag{1}$$

$$k = \frac{u_*^2}{\sqrt{C_\mu}} \tag{2}$$

$$\varepsilon = \frac{u_*^3}{\kappa(z + z_0)} \tag{3}$$

$$\tau = \rho u_*^2 \tag{4}$$

A velocity profile [Eq. (1)] is selected with $u^* = 6.12$ m/s and $z_0 = 2.0$ m. This corresponds to a wind speed of $U_{ref} = 60$ m/s at 100 m height. The roughness length $z_0$ value corresponds to a well-developed urban area where tall buildings are typically located (Blocken, 2015). The inlet $k$ and $\epsilon$ profiles are based on the theoretical Eqs. (2) and (3). The inlet profiles and the modified wall function are implemented in FLUENT with a user-defined function (Abu-Zidan, 2019). The top shear requirement is satisfied by specifying a momentum source term at the topmost cell layer in the domain.

ABL homogeneity is verified by simulating flow in an empty computational domain, and comparing the incident profiles of $U$, $k$, and $\epsilon$ to the inlet profiles. The results are plotted in Figure 2. The incident profiles are plotted at a horizontal distance of $x = 2000$ m from the inlet, which corresponds to the largest upstream fetch used in this study ($l_u = 10H$).

The plots reveal clear conformity between the inlet and incident profiles at all heights in the domain (Figure 2a) and particularly near the ground (Figure 2b). This demonstrates that the inlet profiles are preserved as they travel through the computational domain. In other words, a fully horizontally homogenous atmospheric boundary layer (HHABL) is achieved, and inhomogeneity errors are contained.

### 2.2. Mesh configuration

Another potential source of error in this study is due to spatial discretisation. The impact of this error is mitigated by maintaining a consistent meshing configuration for all simulation cases in this study. This prevents variation in the results that are caused by variation in the mesh (Revuz et al., 2012). To maintain a constant mesh near the building, the larger domain grids are generated by extruding the boundary cells

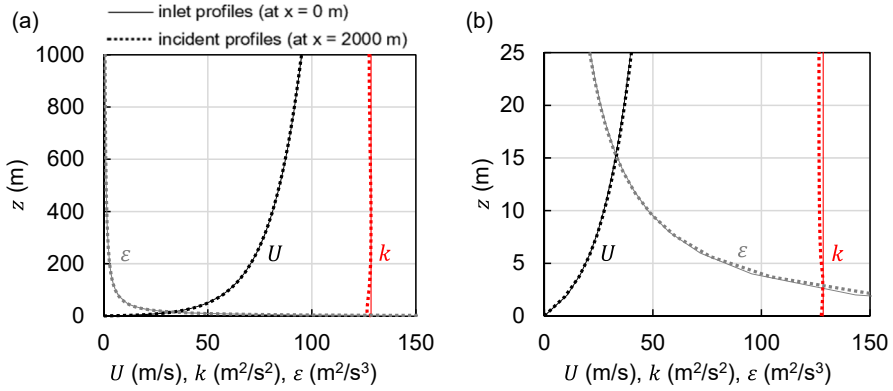


**Figure 2.** Inlet and incident ABL profiles for velocity $U$, turbulence kinetic energy $k$, and turbulence dissipation rate $\epsilon$; from (a) $z = 0$–1000 m; (b) $z = 0$–25 m near the ground surface. $x$ is the streamwise distance from the inlet.

from smaller domains. Furthermore, a grid of high refinement is achieved near the building with structured hexahedron elements. The structured mesh resulted in high-quality elements with skewness <0.5.

To assess the adequacy of the grid, a grid convergence study is performed based on Richardson's extrapolation method (Celik et al., 2008). Three grids of increasing refinement were generated for the base case (BC) in Table (1). The number of elements for the coarse, middle, and fine grid was 1.6, 2.3 and 3.1 million elements respectively. For each of the three grids, results of the building's base reactions and surface pressure along the centreline were obtained. Based on these results, spatial discretisation errors are quantified in terms of the Grid Convergence Index (GCI) (Celik et al., 2008). Spatial discretisation errors for the middle grid were minimal, with GCI values of 0.91% and 0.31% for the base moments and shear respectively, and an average GCI of 0.86% for pressure values extracted along the centreline of the building.

Based on the results of the mesh sensitivity analysis, the middle grid with 2.3 million elements was selected for the BC, with a minimum element size of 0.06 m at the edges of the building, a maximum element size of 50 m at the boundaries of the domain, and an average mesh growth ratio of 1.10. The maximum height of the wall-adjacent elements is 0.07 m at the building surface, and 1.84 m at the ground. The resulting mesh is shown in Figure 3.

### 2.3. Solver settings

Steady-state RANS simulations are performed in CFD code FLUENT with the RNG $k$-$\epsilon$ model. The standard wall function is applied to all surfaces of the building, while the modified wall function is used at the ground boundary. Symmetry boundary conditions are applied to the top and side boundaries of the domain and a pressure outlet condition is specified at the outlet boundary. A pressure-based solver is used with a full pressure-velocity coupling algorithm that solves momentum and continuity equations simultaneously. Spatial discretisation of moment, turbulent kinetic energy, and turbulent dissipation rate is performed using a second-order upwind scheme. A second-order scheme is also used for pressure interpolation, and gradient discretisation is performed using the Least Squares Cell Based method (ANSYS Inc., 2013). The solution is iterated until all scaled residuals dropped below $10^{-5}$. Convergence was verified by monitoring key metrics in the model including base reactions and surface pressure.

## 3. Simulation results and analysis

As previously mentioned, three sensitivity studies are performed in this paper: (1) sensitivity analysis of all four domain extents, (2) sensitivity analysis of the blockage ratio, and (3) analysis of the impact of wind speed and geometric scale. The results of the three sensitivity studies are presented in the following three subsections.

### 3.1. Sensitivity study on the impact domain extents

In the first sensitivity study, the impact of each of the four domain extents, $l_u$, $l_d$, $b$, and $h$, on domain errors is investigated. This is done by varying each dimension in isolation while all other domain dimensions are held at BC values. For instance, when investigating the impact of upstream length, $l_u$ is varied incrementally from 1.5$H$ to 10$H$ (according to Table 1), while $l_d$, $b$, and $h$, are fixed at 15$H$, 5$H$, and 6$H$ respectively.

For each simulation case, pressure coefficients $C_p$ are plotted at the centreline of the windward, leeward, side, and top faces of the building (see Figure 4e). Since a uniform mesh and HHABL conditions are achieved, any variations in the pressure plots can be attributed to variations in the domain size. The pressure coefficients are normalised according to Eq. (5) with $U_H = 70.6$ m/s and $P_{ref} = 0$ Pa for all cases.

$$C_P = \frac{P - P_{ref}}{0.5\rho U_H^2} \tag{5}$$

Figure 4 and Figure 5 show the impact of upstream length $l_u$ and domain width $b$ on surface pressure, respectively. The impact of domain height $h$ and downstream length $l_d$ on surface pressure was minimal even for the smallest dimensions of $h$ and $l_d$ in this study. The maximum percentage error for both dimensions was below 2%. The pressure plots of $h$ and $l_d$ are not presented here as no trends can be visually discerned from the plots.

To further investigate the influence of domain extents on wind load predictions, domain error is calculated as per Eq. (6):

$$Error = \left| \frac{C_P - C_{P\,largest\ domain}}{C_{P\,largest\ domain}} \right| \times 100 \tag{6}$$

where the actual value is assumed to correspond to the largest sized domain corresponding to each of the four domain parameters $l_u$, $l_d$, $b$ and $h$ as listed in Table 1. For instance, the error in Figure 6a is calculated as the deviation of results for cases $l_u$ = 1$H$, 1.5$H$, 2$H$ …etc. from results corresponding to the largest case of $l_u$ = 10$H$. Similarly, errors in Figure 6b for cases $l_d$ = 3$H$, 5$H$, 8$H$ …etc. are calculated as deviations from the largest case of $l_d$ = 25H, and so on. The size of the largest case is exaggerated to ensure that domain error is virtually negligible, which would allow the use of the largest case as a reference for calculating error in the smaller domains.

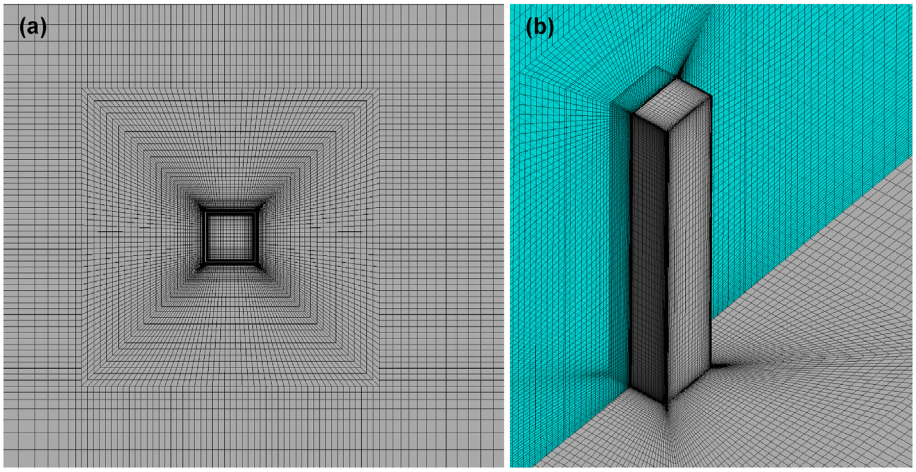


**Figure 3.** (a) Top view and (b) perspective view of structured hexahedral mesh with high refinement near the building.

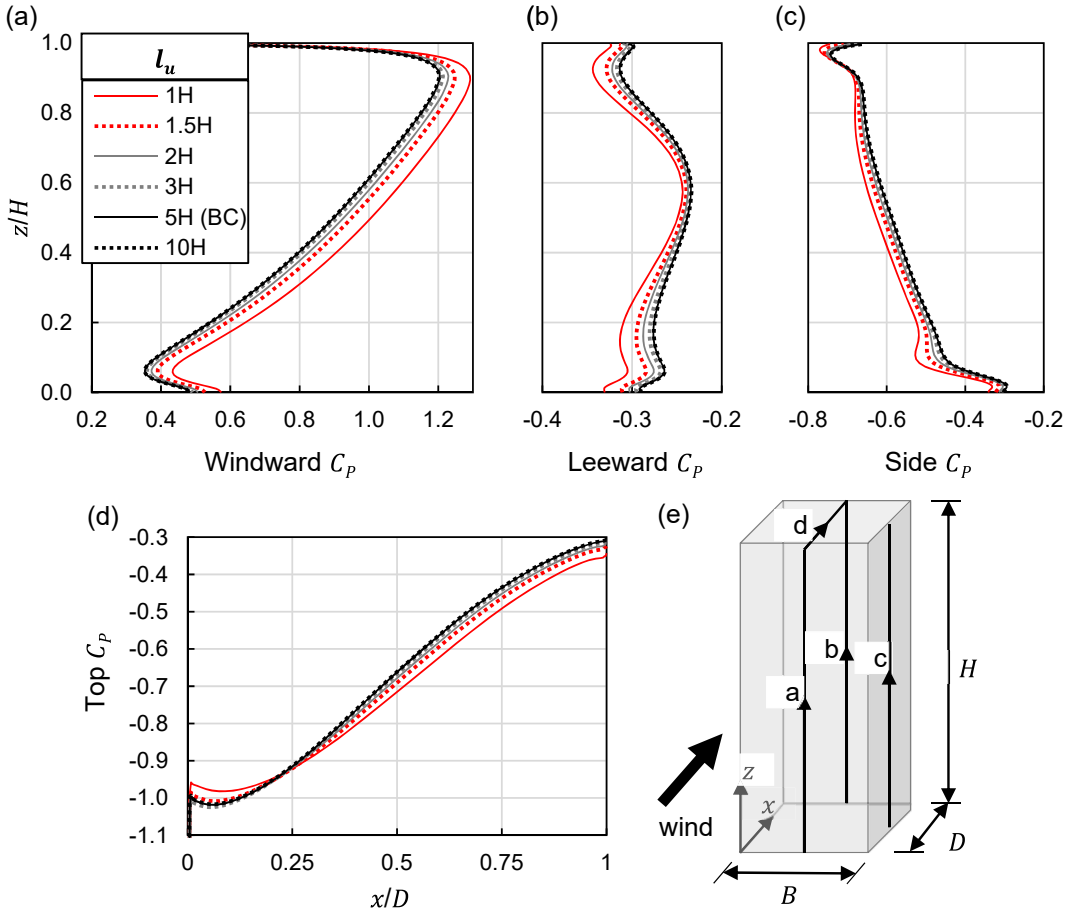


**Figure 4.** Impact of upstream length $l_u$ on surface pressure. $C_p$ plotted along centreline of (a) windward, (b) leeward, (c) side, and (d) top surfaces of building. Plot (e) illustrates the sampling lines in plots (a)–(d), labelled correspondingly.

The following observations are made from the results presented in this section:

- For all four domain dimensions, the error decayed exponentially as the domain is extended in each direction. This behaviour is seen in the error plots in Figure 6. The same behaviour can also be seen, although less apparent, in the pressure plots in Figure 4 and Figure 5 where the pressure profiles converge onto the profiles from the largest domain. This trend justifies the assumption that the large domains in this study are free from domain errors.
- Of the four domain dimensions in this study, the upstream length $l_u$ was found to have the most significant impact on the accuracy of the results. The largest magnitude of error occurred for domains with a short upstream length (Figure 6a). This error occurred on all surfaces of the building but was largest on the windward surface.
- Short upstream lengths resulted in a noticeable increase in pressure on the windward face, and a decrease in pressure on the side, top, and leeward faces of the building (Figure 4). The increase in pressure on the windward face is uniform at all heights of the building. This suggests the absence of ABL inhomogeneity errors, which are largest near the ground and decrease with building height (Abu-Zidan et al., 2020).
- The downstream length $l_d$ had minimal influence on surface pressure. The maximum error was <1.9% for the smallest case of $l_d = 3H$. This error occurred at the leeward face of the building (Figure 6b).
- The domain width $b$ had the second biggest impact on surface pressure; however, these were much smaller than errors due to a short $l_u$. A maximum error of 4.5% occurred for the smallest case of $b = 1.5H$ (Figure 6c). This occurred at the top, leeward, and side faces of the building, while the error on the windward face was less prominent.
- The impact of domain height $h$ was minimal even for the smallest case of $h = 2.2H$ (Figure 6d). The maximum error for all domain height cases was <2%.
- The BC domain size recommended by Franke et al. (2007) was sufficient to ensure negligible impact of domain extents. The maximum domain extent error for the BC was 0.4%, which occurred at the leeward surface of the building.

### 3.2. Sensitivity study on the impact of blockage ratio

The second study examines the impact of the blockage ratio on surface pressure. The blockage ratio (*BR*) refers to the ratio of the projected frontal area of the building to the frontal area of the domain:

$$BR = \frac{frontal\ area\ of\ building}{frontal\ area\ of\ domain} = \frac{B \times H}{h(2b + B)} \tag{7}$$

Since the building dimensions are fixed in this study, the blockage ratio is a function of the domain width $b$ and domain height $h$.

For the *BR* study, a domain length of $l_u = 3H$ and $l_d = 3H$ is selected to reduce computational cost. These values have been shown in Figure 6 to produce minimal domain error. *BR* is varied incrementally from 0.1% to 2.16% by varying $b$ and $h$ simultaneously as per Table 1. The blockage ratio corresponding to the BC is 0.33%.

Once again, $C_P$ values are extracted at the centreline of windward, leeward, side, and top faces of the building (Figure 4e). Error is calculated as variation from the largest domain in the *BR* study with $b = h =$

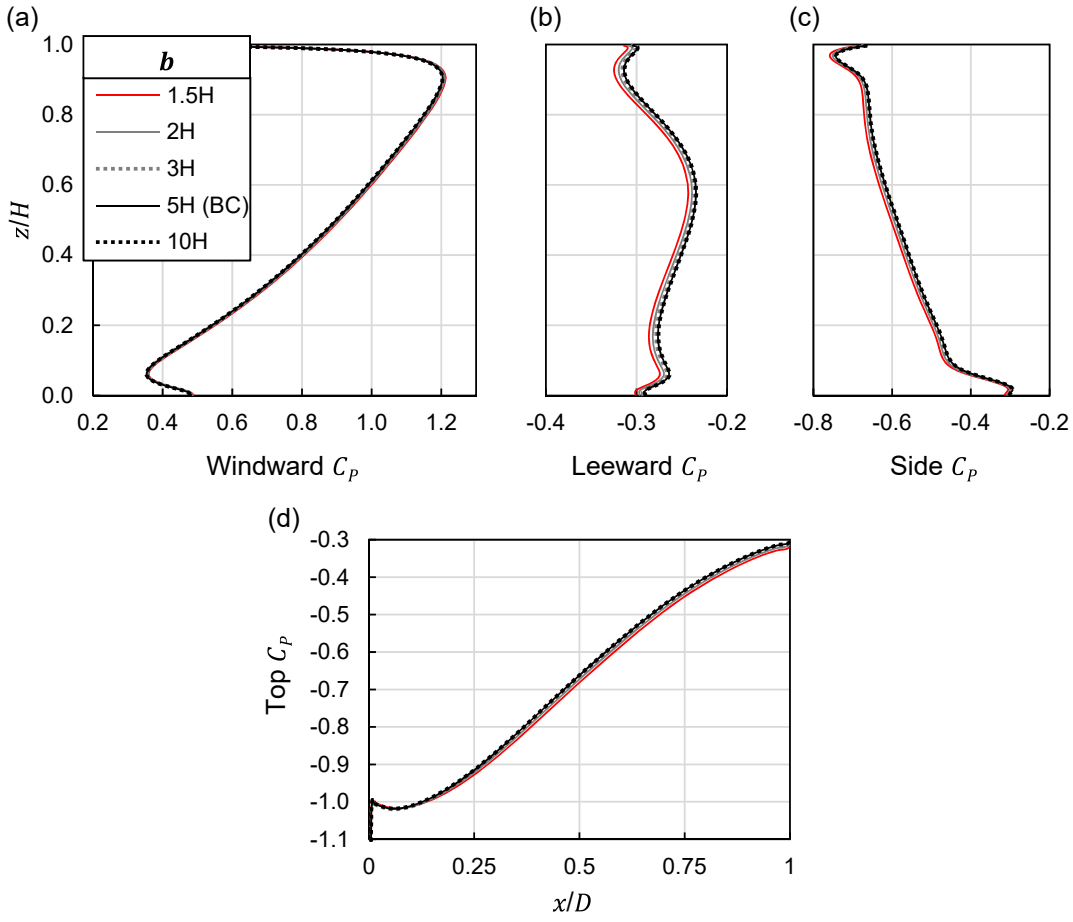


**Figure 5.** Impact of domain width $b$ on surface pressure coefficient $C_P$ along centreline of (a) windward, (b) leeward, (c) side, and (d) top surfaces of building in Figure 4e.

$10H$ ($BR = 0.1\%$). The maximum error due to $BR$ is presented in Figure 7 for each of the building surfaces.

Figure 7 shows that blockage error manifests predominantly on the windward surface of the building, where a higher $BR$ resulted in larger pressures on that surface. This behaviour is comparable to blockage effects observed in wind tunnels (Holmes, 2015). Variations in surface pressure also occur on the leeward, side, and top faces, although these are secondary in magnitude. For the largest blockage ratio case ($BR$ = 2.16%), the maximum error at the windward face was 7.3%, while the maximum error on the other three faces was smaller (1.8%–3.5%).

### 3.3. Sensitivity study on the impact of wind speed and geometric scale

Two additional parameters are investigated for their impact on domain errors; namely the mean wind speed and the geometric scale of the model. These two parameters are analysed for two domain sizes: the BC domain size, and an optimised domain (OD) size that is selected based on the findings from the studies of domain extents and blockage ratio. The dimensions of the OD are selected so that all maximum errors are limited to <4% on all faces. The resulting OD dimensions are $l_u = 3H$, $l_d = 3H$, $b = 3H$, and $h = 4H$, with a corresponding blockage ratio of 0.81%. The OD represents an 87.5% reduction in volume from the BC, and a 40% reduction in mesh count ($1.4 \times 10^6$ in the OD). The maximum $C_P$ error in the OD occurred at the windward surface, with a value of 3.8%.

The impact of wind speed on domain errors is investigated by simulating cases for $U_{ref} = 10$ m/s and $U_{ref} = 60$ m/s in both the BC and the OD. Similarly, the impact of geometric scale on domain errors is investigated with cases at full-scale and 1:400 scale in both the BC and the OD. The resulting windward $C_P$ profiles for the two parameters are shown in Figure 8.

Figure 8 shows that the impact of wind speed and geometric scale on domain errors are almost negligible. The plots for $U_{ref} = 10$ m/s and $U_{ref} = 60$ m/s are identical when performed in similar domain sizes, and the same is true for the full-scale and 1:400 cases. The minor (and almost negligible) variations in the $C_P$ plots occurred mainly due to domain size (i.e. between BC and OD), regardless of the wind speed and geometric scale. This suggests that domain optimisation studies using steady RANS may be performed for any reasonable values of wind speeds and geometric scales.

## 4. Discussion

Based on the results of the sensitivity studies, four main sources of domain errors have been identified: (1) wind-blocking errors due to short upstream length $l_u$, (2) flow recirculation errors due to insufficient downstream length $l_d$, (3) global venturi effects (GVE) due to large blockage ratios, and (4) local venturi effects (LVE) due to insufficient clearance between the building and top and lateral domain boundaries. Each of these is discussed in the following subsections.

### 4.1. Wind-blocking effects

The largest source of domain error in this paper is attributed to the so-called wind-blocking effect that is caused by short upstream distances.

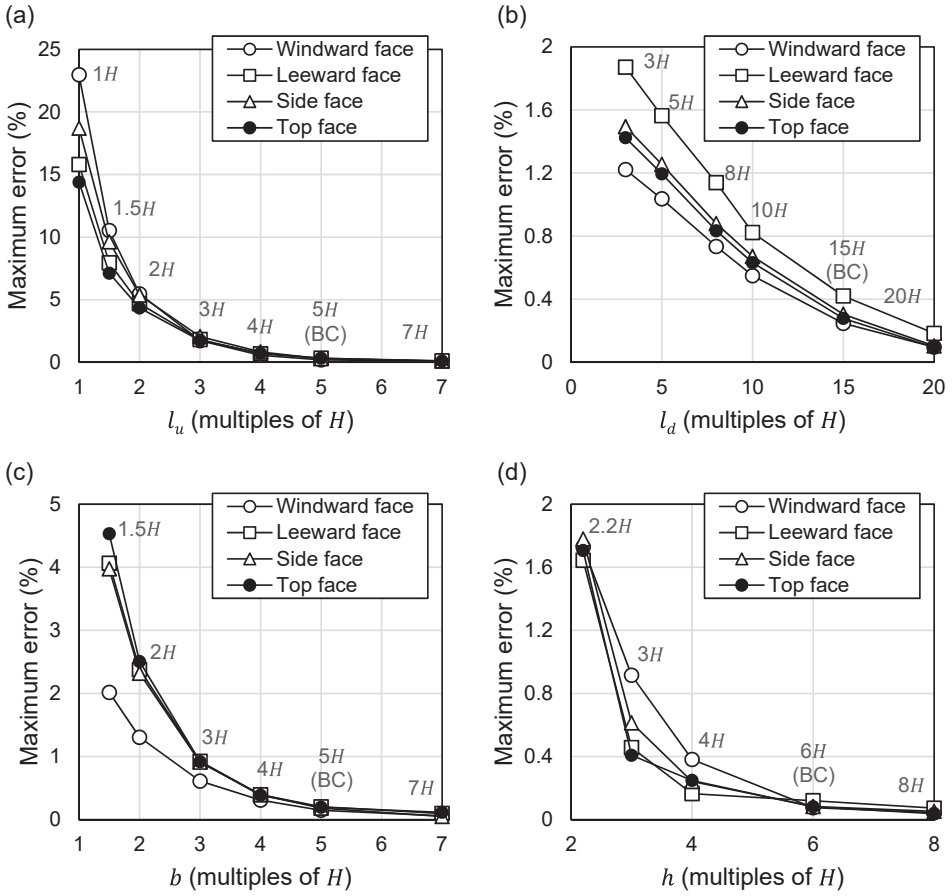


**Figure 6.** Impact of domain extents $l_u$, $l_d$, $b$, and $h$ on domain error of surface pressure. Maximum error (%) computed from centreline $C_P$ at windward, leeward, side, and top building surfaces.

The term wind-blocking effect is used in this paper to refer to "the disturbance of the wind-flow pattern by the presence of the building, and the associated decrease of the upstream stream-wise wind-velocity component near the building" (Blocken and Carmeliet, 2006). This should not be confused with blockage effects that are caused by a large blockage ratio *BR*. The latter will henceforth be termed global venturi effect (GVE) to avoid confusion.

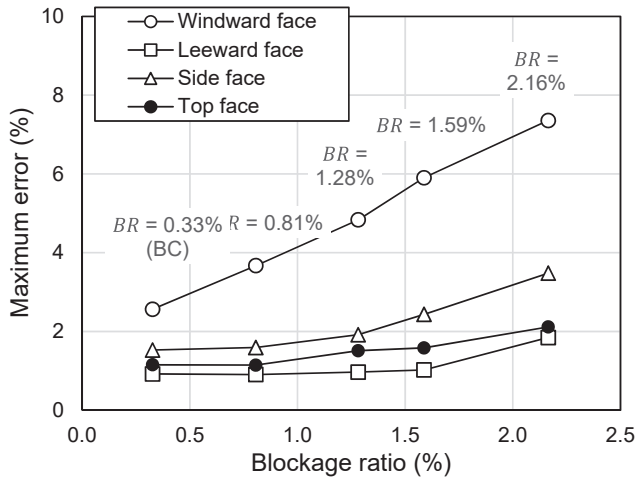


**Figure 7.** Impact of blockage ratio on domain error of surface pressure. Maximum error (%) computed from centreline $C_P$ at windward, leeward, side, and top building surfaces.

Wind-blocking errors arise when the upstream domain length $l_u$ is too short to fully contain the wind-blocking region that forms in front of the building. This results in an interaction between the inlet boundary and the wind-blocking region, as shown in Figure 9a. When the upstream length is too short, the inlet velocity profiles will be imposed at a location where the flow, realistically, ought to slow down and deflect around the building. This causes overprediction of positive pressures on the windward surface (Figure 4a), and overprediction of negative pressures on the leeward, side, and top surfaces (Figure 4b,c,d). Figure 9 shows how increasing $l_u$ allows the wind-blocking region to fully develop.

It is important to note that quantifying wind-blocking error in isolation is not possible without achieving horizontal homogeneity of the atmospheric boundary layer (HHABL). Wind-blocking errors are sensitive to upstream domain length $l_u$, and so too are ABL inhomogeneity errors (Abu-Zidan et al., 2020). If inhomogeneity errors are present in the simulation, then $l_u$ will influence both wind-blocking errors and inhomogeneity errors simultaneously, such that increasing $l_u$ will minimise wind-blocking error while maximising inhomogeneity errors (and vice versa). Demonstrating horizontal homogeneity will confirm that inhomogeneity errors are absent in the simulation which will allow for quantification of domain errors in isolation. To the authors' best knowledge, quantification of wind-blocking errors in isolation has not previously been performed in CFD studies of tall buildings.

### 4.2. Flow recirculation

Flow recirculation error is caused by an insufficient downstream domain length $l_d$, where the outlet boundary interacts with the wake

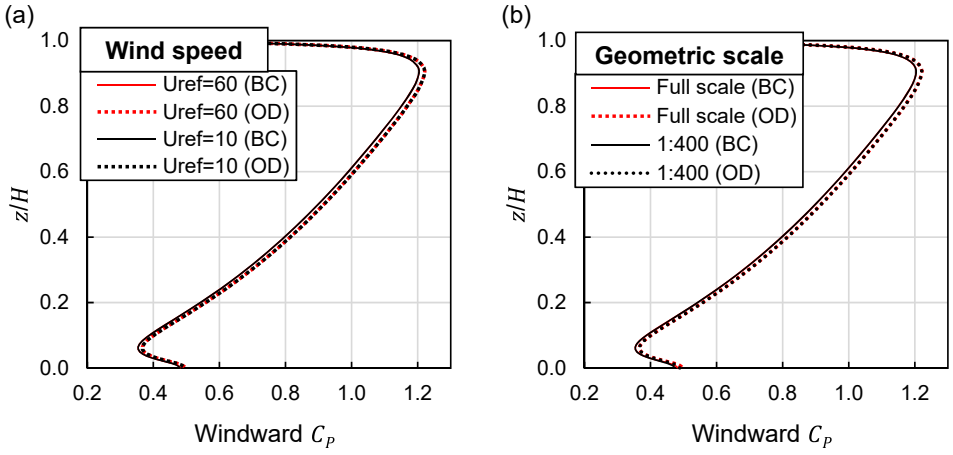


**Figure 8.** Impact of (a) wind speed and (b) geometric scale on windward surface $C_P$.

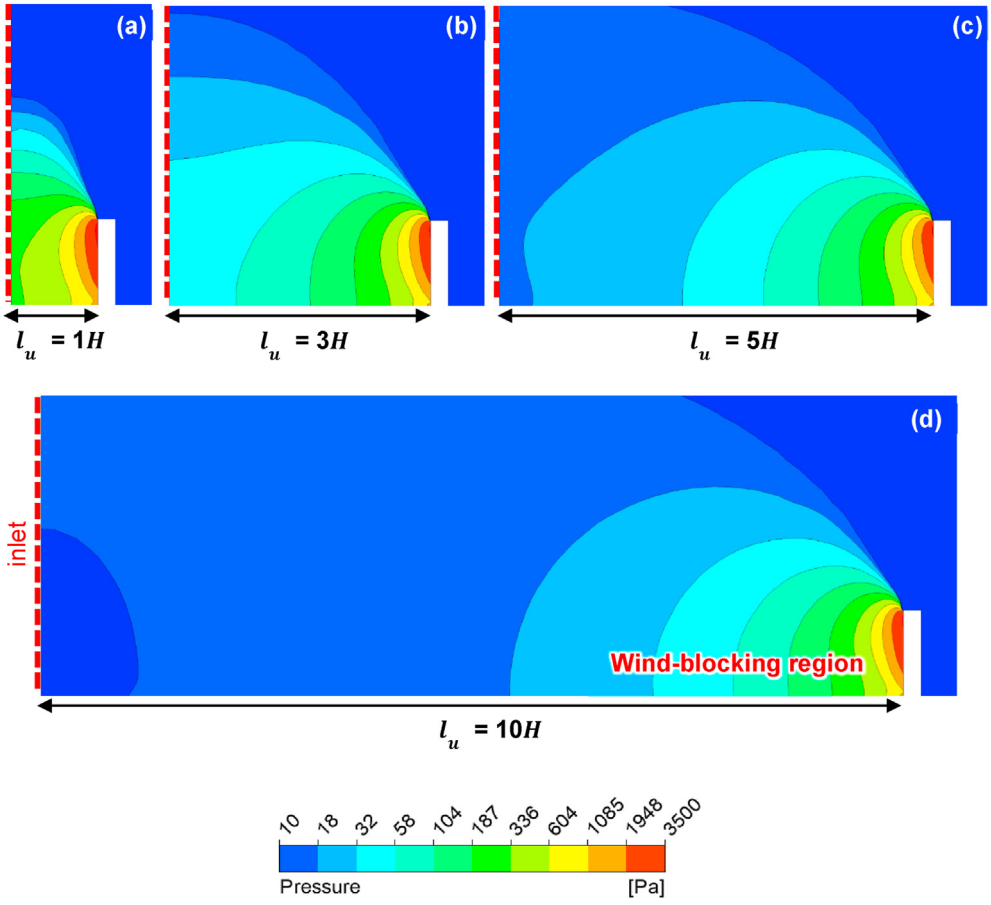


**Figure 9.** Wind-blocking effect visualised with positive pressure contours (log scale) for different upstream lengths $l_u$. Dashed red lines represent location of inlet plane. Flow direction from left to right.

region of the building. This error is often detected during the solution process as it tends to cause numerical instability that prevents convergence. Many CFD codes such as FLUENT alert the user to the presence of recirculation error during the solution process.

Flow recirculation error was insignificant for the domain sizes in this study. Even the smallest $l_d = 3H$ case allowed for full development of the wake region (Figure 10) and resulted in errors of magnitude <2% (Figure 6b). Visual assessment of the wake region (as done in Figure 10) is a crude method for identifying domains that are too short. However, quantification of error may still be required when optimising $l_d$.

The recommended $l_d = 15H$ by Franke et al. (2007) seems overly conservative considering that $l_d = 3H$ was seen to be sufficient in the current study. Nonetheless, larger $l_d$ may still be required in unsteady simulations in order to accurately capture the shedding vortices in the wake (Revuz et al., 2012). Practical experience suggests that shedding vortices in unsteady simulations tend to travel farther downstream compared to the static wake region in steady-state simulations. In such a case, special boundary conditions may be employed to artificially dissipate vortices as they leave the computational domain.

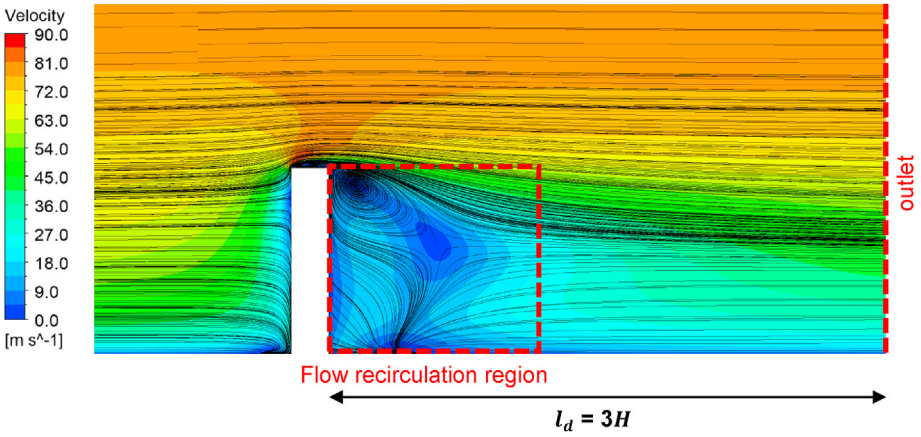


**Figure 10.** Flow recirculation region visualised with velocity contour plots and streamlines. Flow direction from left to right.

### 4.3. Global venturi effects (GVE)

As defined previously, the term global venturi effect (GVE) refers to the commonly cited blockage phenomenon in wind tunnel tests, where global acceleration of flow occurs due to a large blockage ratio (Choi and Kwon, 1998; Holmes, 2015; Takeda and Kato, 1992). This behaviour has also been observed in CFD studies and is considered a primary source of error in small domains (Blocken, 2015; Franke et al., 2007; Revuz et al., 2012).

While GVE errors occur in both CFD and wind tunnel tests, it is important to note that the two may not be equivalent even for the same blockage ratio. This is because the top and side boundaries in CFD do not typically represent the solid walls of the wind tunnel. In some CFD studies, it may be necessary to replicate GVE by sizing the domain according to the cross-sectional dimension of the wind tunnel and treating the top and side boundaries as solid walls (Franke et al., 2007). This may be required in validation studies based on small wind tunnels where blockage effects are inevitable.

GVE errors are controlled by limiting the blockage ratio. In wind tunnel tests, a blockage ratio of $<$ 5–10% is typically allowed (Choi and Kwon, 1998), while CWE guidelines specify a more stringent ratio of $<$3% (Blocken, 2015; Tominaga et al., 2008). The findings of the current study support those by Revuz et al. (2012) that suggest even a smaller blockage ratio for CWE may be required. As shown in Figure 7, the $BR$ = 2.16% case still resulted in a maximum error of 7.3% on the windward face of the building.

### 4.4. Local venturi effects (LVE)

*Local venturi effects (LVE)* are caused by insufficient clearance between the building model and the lateral or top boundaries of the domain. The symmetry condition specified at the top and lateral boundaries is only appropriate if these boundaries are located far from the influence of the building. Otherwise, the symmetry condition will enforce parallel-flow and zero-flux conditions that are non-physical, resulting in flow field errors. These errors are concentrated at the boundaries and propagate inwards towards the building, eventually resulting in surface pressure errors.

Because LVE and GVE are both influenced by the same domain parameters ($b$ and $h$), they are interrelated and often intertwined in an

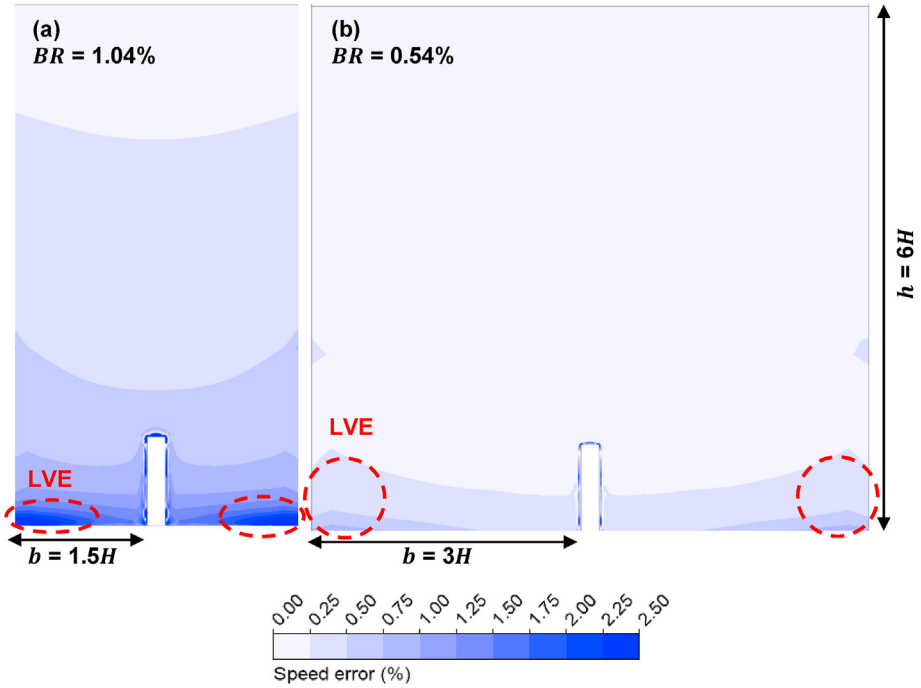


**Figure 11.** Effect of domain width $b$ on flow field errors. Flow direction into page. LVE = local venturi effect.

indecipherable way. Nonetheless, they are two distinct sources of domain error and they impact the results differently. Errors due to LVE dominate in cases of small local clearance and small blockage ratio, while GVE errors dominate in cases with large blockage ratio. The impact of LVE errors on building surface pressure is largest on the side, top, and leeward surfaces of the building (Figure 6c), while GVE errors are largest on the windward surface (Figure 7). To illustrate the differences between LVE and GVE, contour plots of wind speed error are presented in Figure 11, Figure 12, and Figure 13 for the *b*, *h*, and *BR* sensitivity studies, respectively. The contour plots illustrate wind speed error in the cross-sectional plane through the centre of the building, where the direction of flow is into the page.

Figure 11 presents two cases from the domain width study ($b = 1.5H$ and $b = 3H$) where LVE errors are dominant. These errors are concentrated at the side boundaries of the domain. As *b* is increased from $1.5H$ in Figure 11a to $3H$ in Figure 11b, the magnitude of LVE error decreases drastically due to increased side clearance. Nonetheless, LVE remains dominant over GVE in both cases. This is due to the large domain height of $6H$, which ensures a small blockage ratio and prevents GVE errors from dominating.

In Figure 12, two cases from the domain height study are presented ($h = 2.2H$ and $h = 3H$), where the GVE and LVE errors are equally dominant. As the height of the domain is increased from $2.2H$ in Figure 12a to $3H$ in Figure 12b, the magnitude of both LVE and GVE errors decrease. LVE errors drop due to added clearance between the roof of the building and the top boundary, while GVE errors drop due to a reduction in overall *BR*. The equally dominant LVE and GVE errors seen in Figure 12a align with the findings from Figure 6d, where the maximum error on the windward surface due to GVE is roughly the same magnitude as the maximum error on the side, leeward, and top surfaces due to LVE.

Finally, Figure 13 presents three cases from the blockage ratio study that demonstrate the interrelated nature of LVE and GVE. For the case of high $BR = 2.16\%$ in Figure 13a, GVE errors are significant and occur throughout the entire domain cross-section. LVE errors are also present in that case due to the small side and top clearances. As *BR* is reduced to 0.81% in Figure 13b, both GVE and LVE errors significantly drop in magnitude compared to Figure 13a. The colour scale had to be adjusted to visualise the error pattern. As the *BR* is further reduced to 0.33% in Figure 13c, LVE errors significantly drop in comparison to GVE errors, and are no longer visible in the plot. This indicates that for larger domain sizes with small blockage ratios, GVE errors will likely dominate LVE. Hence, domain sizing guidelines based on maximum *BR* may be adequate for controlling both GVE and LVE errors.

## 5. Large-eddy simulation of optimised domain

To extend the findings of this study to unsteady large-eddy simulations (LES), additional cases are performed where LES results from the base case (BC) and optimised domain (OD) are compared. Details of these cases are presented in Table 2.

For each of these cases, unsteady LES is performed with the Dynamic Smagorinsky subgrid model (Lilly, 1992). The segregated algorithm PISO is used for pressure-velocity decoupling (ANSYS Inc, 2013). Momentum terms are discretised using a bounded central differencing scheme, pressure terms are discretised using a second-order scheme, and temporal discretisation is achieved with a bounded second-order implicit scheme. A non-iterative time advancement (NITA) solver is used to reduce computational cost by removing the need for outer iterations.

A mean wind speed of $U_{ref} = 30$ m/s at $z_{ref} = 100$ m is selected, which corresponds to serviceability design wind speed of 25-year return period in Melbourne, Australia (Standards Australia, 2011). Inflow turbulence was ignored to reduce computational cost and to prevent potential inhomogeneity errors that may arise due to the decay of inflow turbulence in the upstream fetch of the domain. A timestep of $\Delta t = 0.01$s is selected which resulted in a maximum courant flow number of less than 5 for the selected grid. The model is solved for 10,000 timesteps (100s) to initialise the solution and then solved for a further 35,000 timesteps (350s) over which instantaneous values of pressure and velocity were averaged. Aside from varying the domain size, all numerical parameters are held constant between the cases to ensure that the influence of domain size is assessed in isolation. The resulting time-averaged $C_P$ profiles for the base case and optimised domain are plotted in Figure 14.

Figure 14a demonstrates that the optimised domain was able to accurately replicate the windward pressure profiles of the base case, where the average deviation between the two cases was 0.8%. On the leeward and side faces, however, Figures 14b,c show that the optimised domain resulted in a noticeable overprediction of negative pressure compared to the base case, where the average deviation on the leeward and side faces was 10.7% and 7.7%, respectively.

To investigate the cause of this discrepancy, a third case (case 3) is performed with an upstream length $l_u$ equivalent to that of the base case, and all other domain dimensions equivalent to the optimised domain. The results, also plotted in Figure 14, show close agreement to those of the base case, where the average deviation on the windward, leeward, and side faces was 0.1%, 3.7%, and 1.1%, respectively. This suggests that the primary cause of discrepancies in the results from the OD and BC is due to differences in upstream domain length $l_u$, but it is unclear whether these variations are caused by the wind-blocking effect observed in steady RANS results. It is also unclear whether optimisation of $l_u$ using steady RANS could potentially translate to unsteady LES. Further research is needed to study the influence of upstream domain length on LES results.

Nonetheless, the results of this study suggest that steady RANS can be effective for optimising the height *h*, width *b*, and downstream length $l_d$ of the domain for use in LES. Optimising these parameters resulted in a 50% reduction of computational time compared to the base case.

## 6. Framework for domain optimisation study

The findings of this study indicate that domain sizing guidelines by Franke et al. (2007), although sufficient for eliminating domain errors, are exceedingly conservative when applied to tall building simulations. Optimising the domain size is strongly recommended as it can lead to significant reduction in mesh size and computational cost. These savings become critical when performing unsteady simulations that involve thousands of timesteps.

Domain size optimisation is highly problem-specific and depends on multiple factors that include the building geometry and orientation, as well as the acceptable level of error for the application of interest. This level of complexity is difficult to codify. Hence, instead of providing specific sizing guidelines, this section proposes a general framework for optimising the computational domain size:

### 6.1. Aim and requirements of domain optimisation study

The aim of a domain size optimisation study is to identify the smallest possible domain size for which domain error remains within the acceptable tolerance. Domain errors are estimated by comparing variables of interest of the optimised domain with corresponding values in an excessively large domain. When setting up a domain optimisation study, the following requirements should be taken into consideration:

- Domain errors should be assessed in isolation from other sources of error. Thus, ABL homogeneity is a critical requirement. HHABL conditions can be achieved in FLUENT for RNG $k$-$\epsilon$ model by adopting the approach described by Abu-Zidan et al. (2020). Moreover, mesh variation between the different domain sizes should be limited, particularly near the building model. For irregular geometries and

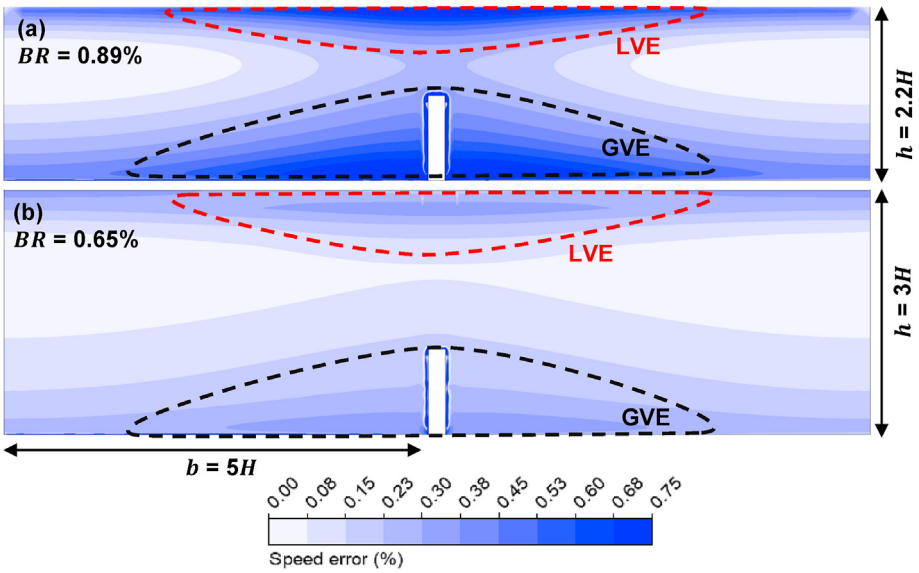


**Figure 12.** Effect of domain height on flow field errors. Flow direction into page. LVE = local venturi effect; GVE = global venturi effect.

unstructured grids, this can be achieved with a nested meshing approach.

- Proper convergence of the solution is critical in domain optimisation studies as error due to unconverged results can be significant. Negative pressures on the side and leeward building surfaces are particularly volatile, requiring many iterations before reaching convergence. Solution convergence should be verified by monitoring variables of interest during the solution process.
- Wind velocity and geometric scale were found to have minimal impact on domain errors for steady RANS. Hence, domain optimisation studies can be performed for any reasonable wind speed profile and geometric scale.

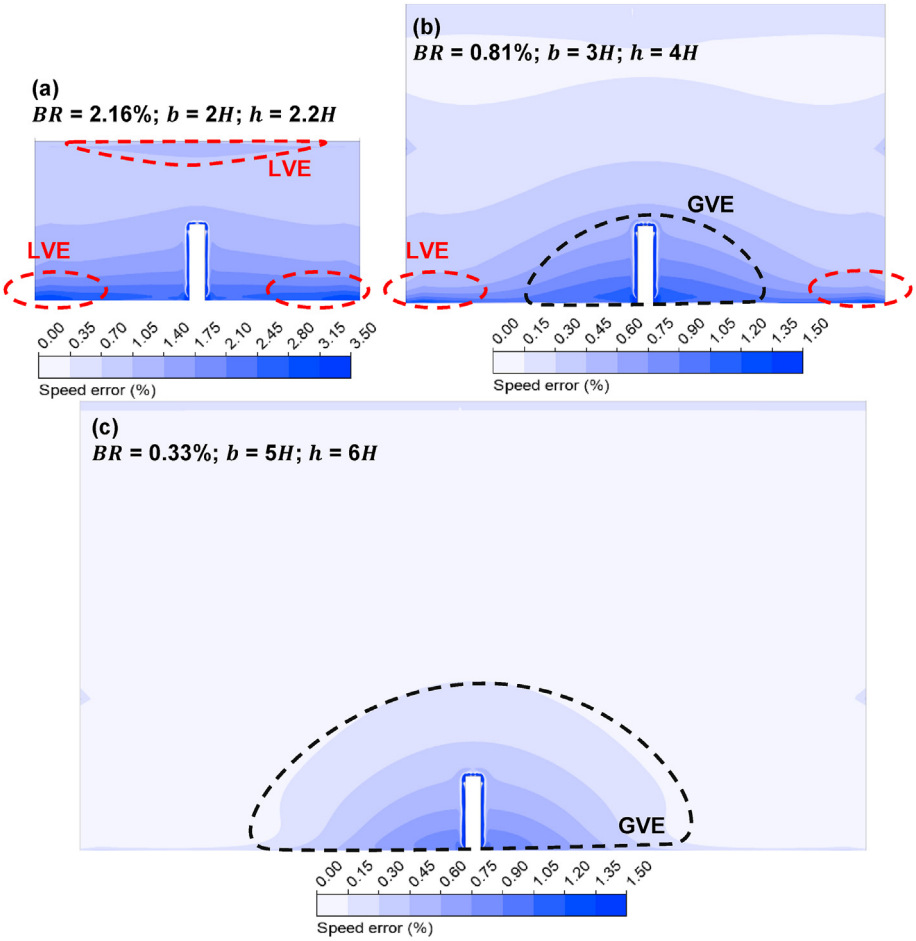


**Figure 13.** Effect of blockage ratio on flow field errors. Flow direction into page.

**Table 2.** Details of LES cases.

| | Case 1 (BC) | Case 2 (OD) | Case 3 |
|---|---|---|---|
| $l_u$ | 5$H$ | 3$H$ | 5$H$ |
| $l_d$ | 15$H$ | 3$H$ | 3$H$ |
| $b$ | 5$H$ | 3$H$ | 3$H$ |
| $h$ | 6$H$ | 4$H$ | 4$H$ |
| Cell count ($\times 10^6$) | 2.3 | 1.4 | 1.5 |

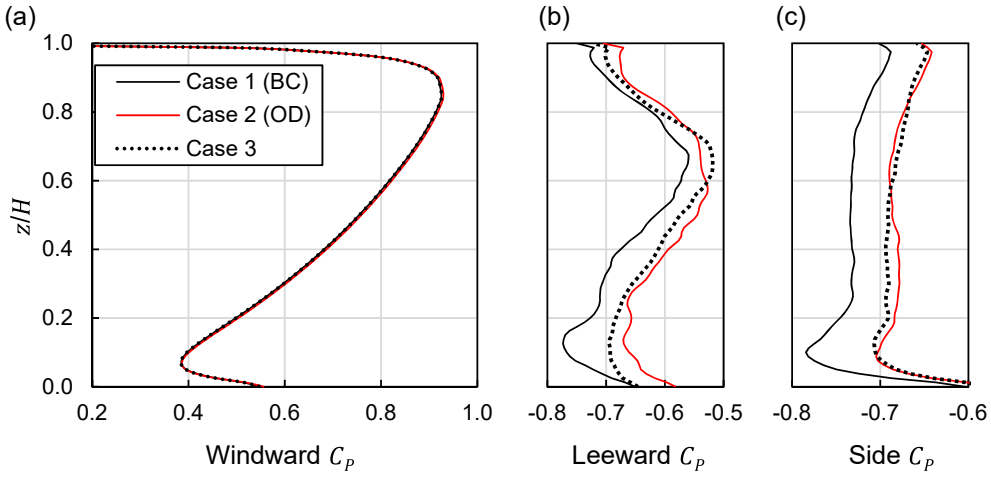


**Figure 14.** Comparison of LES results for base case (BC) and optimised domain (OD).

### 6.2. Optimising the domain dimensions

The domain size is optimised based on sensitivity studies that involve parametrising each of the four domain dimensions ($l_u$, $l_d$, $b$, and $h$). Appropriate domain dimensions are then selected based on the acceptable level of domain error in the variables of interest.

- ***Selecting upstream length*** $l_u$
  An adequate upstream domain length should be selected to limit the magnitude of wind-blocking errors. $l_u$ can vary with building geometry and orientation, as these parameters affect wind-blockage (Blocken and Carmeliet, 2006). The greater the wind-blocking effect and the further upstream it propagates, the larger the requirement of $l_u$. Upstream length can have a substantial impact on computational cost in unsteady simulations where high mesh refinement in the upstream region is required to ensure an accurate transfer of inflow turbulence from the inlet boundary to the building. It is unclear from the findings of this study whether optimisation of $l_u$ using steady RANS will sufficiently translate to unsteady LES. This is an area for future research.
- ***Selecting downstream length*** $l_d$
  The downstream length has a significant impact on computational cost since a high mesh refinement is required in the wake region to capture complex flow features. An adequate $l_d$ should be provided to ensure that the outflow boundary is sufficiently distant from the wake region, thus minimizing flow recirculation errors. In this study, an optimised value of $l_d = 3H$, determined using steady RANS, was found to be sufficient for unsteady LES.
- ***Selecting domain width*** $b$ ***and height*** $h$
  Conservative values for $b$ and $h$ may be selected since these do not significantly influence computational cost. This is because mesh refinement is not required at the lateral and top extents of the domain. For the rectangular building in this study, a maximum blockage ratio of <1% is recommended. This stringent value would ensure that both GVE and LVE errors are contained within acceptable limits. Nonetheless, it may be worthwhile verifying the absence of these errors with sensitivity studies.

## 7. Conclusion

This paper investigates the effect of computational domain size on CFD predictions of wind loads on tall buildings. Four distinct sources of domain error are identified which include wind-blocking errors caused by short upstream length, flow recirculation errors due to insufficient downstream length, global venturi effects (GVE) due to large blockage ratios, and local venturi effects (LVE) caused by insufficient clearance between the building and top and lateral domain boundaries. Domain errors were found to be significant for domains with a short upstream fetch and large blockage ratio, and these errors can significantly compromise the reliability of the solution. A framework for optimizing domain size in building studies is proposed which involves parametrizing the domain dimensions and performing sensitivity study on variables of interest. The findings and recommendations of this paper are intended to assist the modelling process for practitioners and result in more computationally efficient and reliable CFD simulations for tall buildings.

## Declarations

### Author contribution statement

Yousef Abu-Zidan: Conceived and designed the experiments; Performed the experiments; Analyzed and interpreted the data; Contributed reagents, materials, analysis tools or data; Wrote the paper.

Priyan Mendis & Tharaka Gunawardena: Conceived and designed the experiments; Wrote the paper.

*Funding statement*

This research was supported by the Cooperative Research Centres Projects Round 8 Grant CRCPEIGHT000084: Upcycling solutions for hazardous claddings and co-mingled waste, the Australian Research Council Industrial Transformation Research Programme IC150100023: ARC Training Centre for Advanced Manufacturing of Prefabricated Housing, and an Australian Government Research Training Program (RTP) Scholarship.

*Data availability statement*

Data will be made available on request.

*Declaration of interests statement*

The authors declare no conflict of interest.

*Additional information*

No additional information is available for this paper.

## References

Abu-Zidan, Y., 2019. Verification and Validation Framework for Computational Fluid Dynamics Simulation of Wind Loads on Tall Buildings. Department of Infrastructure Engineering. The University of Melbourne.

Abu-Zidan, Y., Mendis, P., Gunawardena, T., 2020. Impact of atmospheric boundary layer inhomogeneity in CFD simulations of tall buildings. Heliyon 6, e04274.

Ai, Z.T., Mak, C.M., 2015. Large-eddy Simulation of flow and dispersion around an isolated building: analysis of influencing factors. Comput. Fluid 118, 89–100.

ANSYS Inc, 2013. ANSYS Fluent Theory Guide, USA.

Baetke, F., Werner, H., Wengle, H., 1990. Numerical simulation of turbulent flow over surface-mounted obstacles with sharp edges and corners. J. Wind Eng. Ind. Aerod. 35, 129–147.

Blocken, B., 2015. Computational Fluid Dynamics for urban physics: importance, scales, possibilities, limitations and ten tips and tricks towards accurate and reliable simulations. Build. Environ. 91, 219–245.

Blocken, B., Carmeliet, J., 2006. The influence of the wind-blocking effect by a building on its wind-driven rain exposure. J. Wind Eng. Ind. Aerod. 94, 101–127.

Braun, A.L., Awruch, A.M., 2009. Aerodynamic and aeroelastic analyses on the CAARC standard tall building model using numerical simulation. Comput. Struct. 87, 564–581.

Buccolieri, R., Di Sabatino, S., 2007. Flow and pollutant dispersion in urban arrays for the standardization of CFD modelling practise. In: 11th International Conference on Harmonisation within Atmospheric Dispersion Modelling for Regulatory Purposes, Cambridge.

Castro, I.P., Cowan, I.R., Robins, A.G., 1999. Simulations of flow and dispersion around buildings. J. Aero. Eng. 12, 145–160.

Celik, I.B., Ghia, U., Roache, P.J., Freitas, C.J., Coleman, H., Raad, P.E., 2008. Procedure for estimation and reporting of uncertainty due to discretization in CFD applications. J. Fluid Eng. 130, 078001–078001-078004.

Choi, C.K.K., Kwon, D.K., 1998. Wind tunnel blockage effects on aerodynamic behaviour of bluff body. Wind Struct. 1, 351–364.

Cowan, I.R., Castro, I.P., Robins, A.G., 1997. Numerical considerations for simulations of flow and dispersion around buildings. J. Wind Eng. Ind. Aerod. 67–68, 535–545.

Franke, J., Hellsten, A., Schlünzen, H., Carissimo, B., 2007. Best Practice Guideline for the CFD Simulation of Flows in the Urban Environment. COST Office, Brussels.

Hall, R.C., 1997. Application of Computational Fluid Dynamics to Near-Field Atmospheric Dispersion, Atmospheric Dispersion Modelling Liaison Committee Annual Report 1995-1996 (Annex B), Chilton.

Holmes, J.D., 2015. Wind Loading of Structures. CRC Press.

Huang, M.F., Lau, I.W.H., Chan, C.M., Kwok, K.C.S., Li, G., 2011. A hybrid RANS and kinematic simulation of wind load effects on full-scale tall buildings. J. Wind Eng. Ind. Aerod. 99, 1126–1138.

Huang, S., Li, Q.S., Xu, S., 2007. Numerical evaluation of wind effects on a tall steel building by CFD. J. Constr. Steel Res. 63, 612–627.

Lilly, D.K., 1992. A proposed modification of the Germano subgrid-scale closure method. Physics of Fluids A: Fluid Dynam. 4, 633–635.

Parente, A., Gorlé, C., van Beeck, J., Benocci, C., 2011. Improved k–ε model and wall function formulation for the RANS simulation of ABL flows. J. Wind Eng. Ind. Aerod. 99, 267–278.

Ramponi, R., Blocken, B., 2012. CFD simulation of cross-ventilation for a generic isolated building: impact of computational parameters. Build. Environ. 53, 34–48.

Revuz, J., Hargreaves, D.M., Owen, J.S., 2012. On the domain size for the steady-state CFD modelling of a tall building. Wind Struct. 15, 313–329.

Ricci, M., Patruno, L., Kalkman, I., de Miranda, S., Blocken, B., 2018. Towards LES as a design tool: wind loads assessment on a high-rise building. J. Wind Eng. Ind. Aerod. 180, 1–18.

Richards, P.J., Norris, S.E., 2011. Appropriate boundary conditions for computational wind engineering models revisited. J. Wind Eng. Ind. Aerod. 99, 257–266.

Standards Australia, 2011. Structural Design Actions. Part 2: Wind Actions, AS/NZS 1170.2:2011. Standards Australia. New South Wales, Sydney.

Takeda, K., Kato, M., 1992. Wind tunnel blockage effects on drag coefficient and wind-induced vibration. J. Wind Eng. Ind. Aerod. 42, 897–908.

Tominaga, Y., Mochida, A., Yoshie, R., Kataoka, H., Nozu, T., Yoshikawa, M., Shirasawa, T., 2008. AIJ guidelines for practical applications of CFD to pedestrian wind environment around buildings. J. Wind Eng. Ind. Aerod. 96, 1749–1761.

Xiang, W.Z., Wang, H.S., 2007. Discussion on Grid Size and Computational Domain in CFD Simulation of Pedestrian Wind Environment Around Buildings, Building Simulation, Beijing, China, p. 1150.

Zhang, Y., Habashi, W.G., Khurram, R.A., 2015. Predicting wind-induced vibrations of high-rise buildings using unsteady CFD and modal analysis. J. Wind Eng. Ind. Aerod. 136, 165–179.